Materials Science & Engineering A 581 (2013) 39–47

Contents lists available at SciVerse ScienceDirect

Materials Science & Engineering A

journal homepage: www.elsevier.com/locate/msea

Static recrystallization of strip cast alloys in the presence of complex nano-sulfide and nitride precipitates

Shokoufeh Malekjani *, Ilana. B. Timokhina, Jiangting Wang, Peter D. Hodgson, Nicole E. Stanford

Institute for Frontier Materials, Deakin University, Waurn Ponds, VIC 3216, Australia

ARTICLE INFO

Article history:
Received 11 February 2013
Received in revised form
17 May 2013
Accepted 28 May 2013
Available online 5 June 2013

Keywords:
Strip casting
Rapid solidification
Steel
Recrystallization
Zener pinning

ABSTRACT

The static recrystallization of three strip cast stainless steels including one ferritic stainless steel, one austenitic stainless steel and a 201 stainless steel was investigated in the present work. The samples were obtained from a laboratory scale strip casting simulator and were subjected to cold rolling and annealing. It is shown that the strip cast samples develop nano-precipitates which in the case of austenitic and ferritic stainless steels can significantly hinder the recrystallization kinetics. Two different precipitate species were identified: sulfides and nitrides. The sulfides are formed in the as-cast structure and hinder recrystallization. These can be coarsened by heat treatment to make recrystallization more rapid. The nitrides, however, are in solution in the as-cast condition and only retard the recrystallization after a heat treatment has been used to cause their precipitation.

1. Introduction

Strip casting is a continuous casting process with the capability of producing near net shape products allowing cost, energy and environmentally efficient steel production. Direct strip casting solidifies steel directly into thin sheet of ~2 mm in thickness, and the elimination of intermediate hot rolling steps can reduce energy consumption by up to 90% [1]. Strip casting subjects the steel to uniquely high cooling rates, many hundreds of degrees per second [1,2]. Consequently, strip cast steels have very different microstructures compared to conventional sheets produced by thermo-mechanical processing. The rapid cooling experienced during strip casting can produce super saturated solid solutions, and has also been reported to form nano-precipitates and solute clusters [3–7]. In the former case, fine particles are known to have a significant impact on the recrystallization of alloys due to Zener pinning of moving grain boundaries [8–10], and this is the topic of the present work.

Of interest in the present paper is the static recrystallization behavior of strip cast steels after cold rolling. There have been some reports of retarded recrystallization kinetics in strip cast steels compared to conventionally processed materials [6,11,12]. Xu and Ferry [11] reported delayed recrystallization after strip casting in a low carbon steel, and Arribas et al. [12] reported that TiN particles developed during rapid solidification were effective in retarding the static and dynamic recrystallization of a low carbon steel. Frawley et al. [6] have also reported the inhibition of austenite recrystallization in low carbon steel as a result of fine Mn and Cu sulfide particles developing during thin slab casting. From this limited number of published papers, there seems to be compelling evidence that, firstly, fine particles can develop during rapid solidification of low carbon steels and, secondly, that these particles are able to retard recrystallization. Although this has been found to be the case for plain carbon steel grades, there is no information about how these particles may affect other steel grades. Consequently, we present here a dedicated study on the effect of strip casting on the recrystallization behavior of three different stainless steel alloys: one ferritic steel, one austenitic steel, and a 200 series alloy that is duplex in nature after strip casting. Since we now know that particles can have a major effect on recrystallization, a significant part of this research will be to identify the different particles that develop and determine how they behave during processing.

2. Experimental work

Three different alloys were used in this study with the chemical composition given in Table 1. The samples were obtained from a laboratory scale strip casting simulator known as a dip tester.

* Corresponding author. Tel.: +61 3 5227 2350; fax: +61 3 5227 1103.
E-mail addresses: s.malekjani@deakin.edu.au (S. Malekjani), ilana.timokhina@deakin.edu.au (Ilana. B. Timokhina), Jiangting.wang@deakin.edu.au (J. Wang), peter.hodgson@deakin.edu.au (P.D. Hodgson), nicole.stanford@deakin.edu.au (N.E. Stanford).

0921-5093/$ - see front matter © 2013 Elsevier B.V. All rights reserved.
http://dx.doi.org/10.1016/j.msea.2013.05.070

Table 1
Chemical composition (wt%) of alloys used in this study.

Alloy type	C	Mn	Cr	Ni	Al	Si	N	S	P	Fe
Fe–18Cr–5Ni–6Mn (AISI 201 series)	0.11	6.0	17.7	4.8	0.15	0.77	0.20	0.017	0.007	Bal
Fe–15Cr–4Al (Ferritic stainless steel)	0.04	0.2	15.3	0.3	3.74	0.43	0.14	0.009	0.010	Bal
Fe–35Ni (Austenitic stainless steel)	0.02	0.3	–	35.2	0.03	0.19	0.10	0.014	0.015	Bal

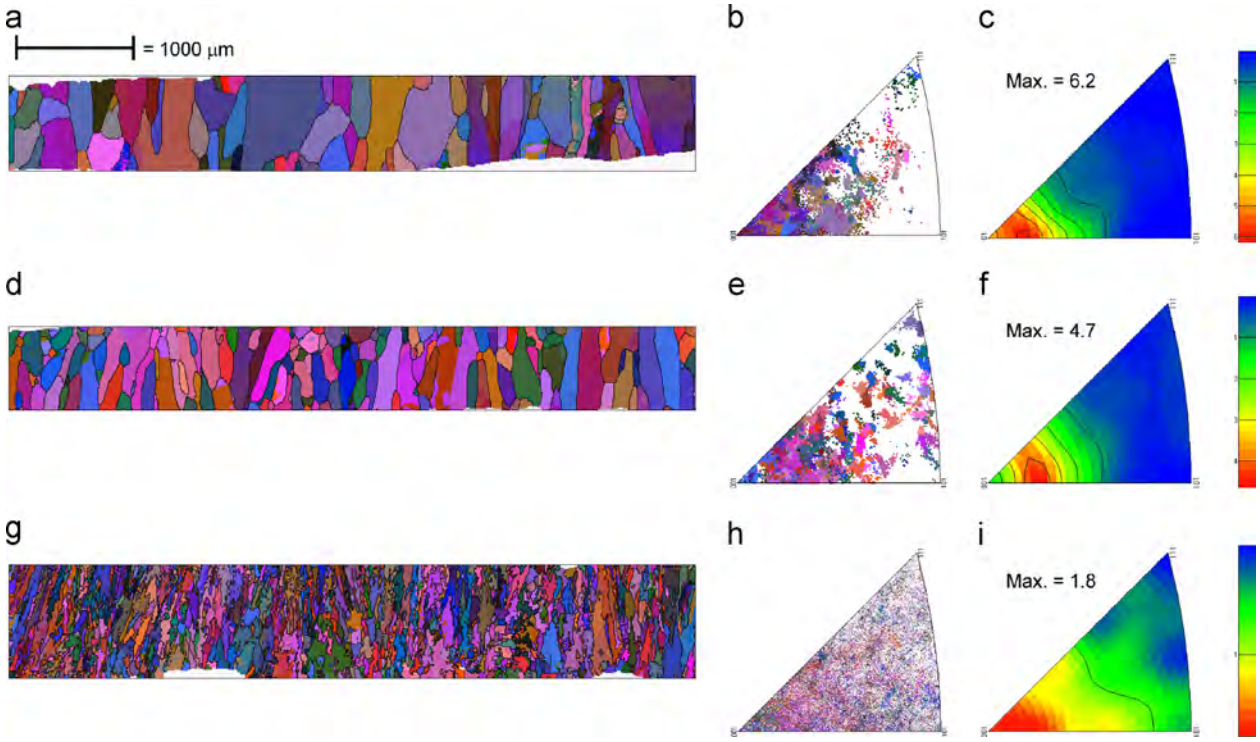

Fig. 1. Microstructural images and corresponding inverse pole figures of as cast. (a–c) Ferritic stainless steel, (d–f) Austenitic stainless steel, (g–i) 201 stainless steel. The black arrows show the solidification direction and the upper surface is the substrate surface.

This design has been described in detail previously [13] and will only briefly be described here. The dip tester is a rapid solidification simulator which is used to immerse a copper substrate into molten steel for a short and controlled period of time. The substrate is immediately retracted from the furnace and the sample removed from the substrate. The samples have dimensions of 35×35 mm^2, and a thickness that varies between 0.5 and 1 mm depending on the alloy, melt temperature and residence time of the substrate in the liquid steel. The specifics of the melt practice for each of the three materials tested here can be found in Refs. [14-16].

The cast samples were cut into strips approximately 10 mm wide, and then cold rolled to ~60% reduction in 5–8 passes. To study the recrystallization kinetics the cold rolled samples were subjected to annealing at 850 °C in a fluid bed furnace. The holding time varied between 5 s and 1800 s. For the 201 stainless steel samples, the recrystallization kinetics were also studied at 750 °C due to rapid recrystallization at 850 °C.

To effectively compare the recrystallization behavior of the strip cast samples to that which would be expected from a conventionally cast sample, a second set of samples were subject to simulated coiling. The purpose of this treatment was to simulate the temperatures and times that may be used during hot rolling and coiling of conventional product, processes which modify the carbides, sulfides and nitrides that may be present in the steel. The simulated coiling procedure was a 1 h hold at 1000 °C followed by slow cooling to 550 °C for an additional 3 h hold.

The microstructural investigations were performed using a LEO 1530, Supra 55 VP and Quanta FEG scanning electron microscopes (SEM). SEM was used to characterize the microstructure using angular selective back-scatter (AsB) imaging and electron back-scatter diffraction (EBSD). Recrystallization fraction was calculated utilizing images obtained by AsB and point counting method. Transmission electron microscopy (TEM) was carried out with a 2001F field emission gun TEM equipped with a JEOL energy dispersive spectroscopy (EDS) system for compositional mapping.

3. Results

3.1. As cast microstructure

The microstructure of the as-cast samples are shown in Fig. 1. For the ferritic and austenitic steels, which do not undergo a solid state phase transformation during cooling, the as-cast structure is retained at room temperature. The grains nucleate on the copper substrate, and grow toward the melt during the immersion. The grains are in the range between 60–150 μm wide and 500–1000 μm long, and are typical for this kind of alloy [17]. The corresponding inverse pole figures are shown in Fig. 1b and c, and show a preference for 001 poles to be aligned in the solidification direction. This is consistent with this being the preferred growth direction of solid from liquid [18]. The austenitic stainless steel is also a composition that does not undergo a

solid state phase transformation on cooling, and consequently develops a very similar microstructure and texture to the ferritic grade, Fig. 1d–f. However, the 201 stainless steel shows a markedly different microstructure. This alloy solidifies as delta ferrite and transforms into austenite during cooling, and this is commensurate with a significant refinement in the grain size and a weakening of the texture, Fig. 1g–i. Although at equilibrium the alloy is fully austenitic, the rapid solidification resulted in some solute segregation of Cr in the inter-dendritic regions which stabilised delta ferrite, Figs. 2a and 3a. This alloy was therefore a duplex material after strip casting.

Transmission electron microscopy (TEM) revealed some small particles in the steels (Figs. 4 and 5), and a summary of the observed size range of particles is given in Table 2. In all cases the particles were identified chemically using EDS mapping, and found to be associated with sulfur. For the case of the austenitic steel the sulfides had a simple chemistry of Mn and S. However the ferritic alloy, probably due to its high Al concentration, formed complex nitro-sulfides.

3.2. Coiled microstructure

Transmission electron microscopy of the ferritic and austenitic steels revealed significant coarsening of the particles as a result of the simulated coiling, Fig. 6, and Table 2. For the 201 stainless alloy the coiling treatment coarsened the existing sulfide particles, and caused the precipitation of aluminum nitrides that were not observed in the as-cast condition, Figs. 2 and 5.

The as-cast 201 stainless steel exhibited inter-dendritic delta ferrite, as stated earlier. After the simulated coiling the inter-dendritic regions were dissolved and no longer present in the microstructure, Fig. 3b. The coiling also caused some grain growth, Fig. 7. There were no significant changes in the grain size or shape of the ferritic and austenitic alloys after simulated coiling.

3.3. Cold rolled and annealed microstructure

To investigate the recrystallization response of the as-cast samples, a series of cold rolling and annealing experiments were performed on the as-cast samples. All three samples showed a typical cold rolled microstructure consisting of elongated grains in the rolling direction.

Fig. 8 shows the microstructure of the partially recrystallized samples. For the austenitic and ferritic samples, the nucleation was inhomogeneous through-out the microstructure, with the grain boundaries acting as preferred nucleation sites for recrystallization. Some nucleation from within the large deformed grains was

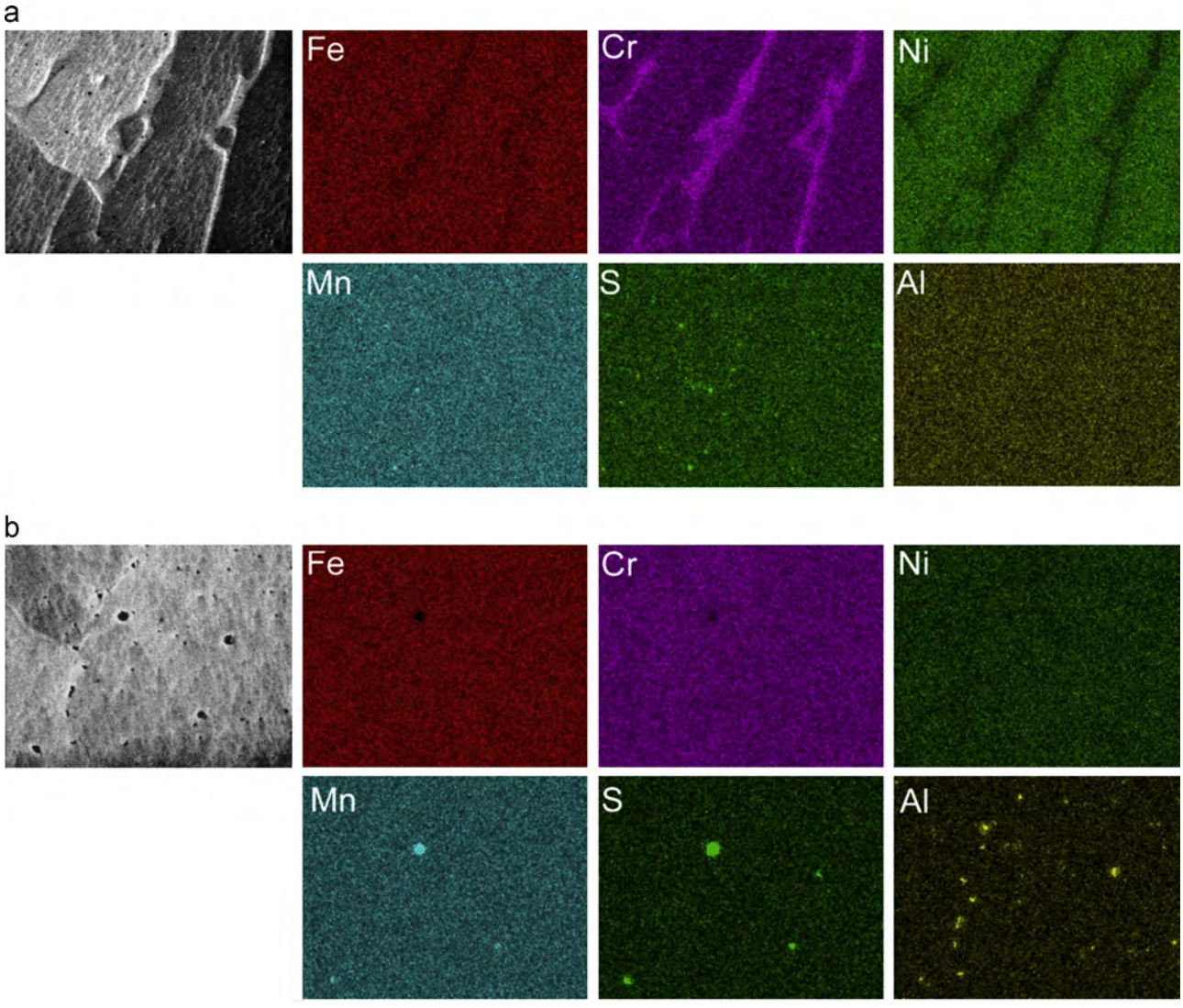

Fig. 2. Composition mapping using EDS of the 201 stainless steel and (a) the as-cast condition and (b) after simulated coiling.

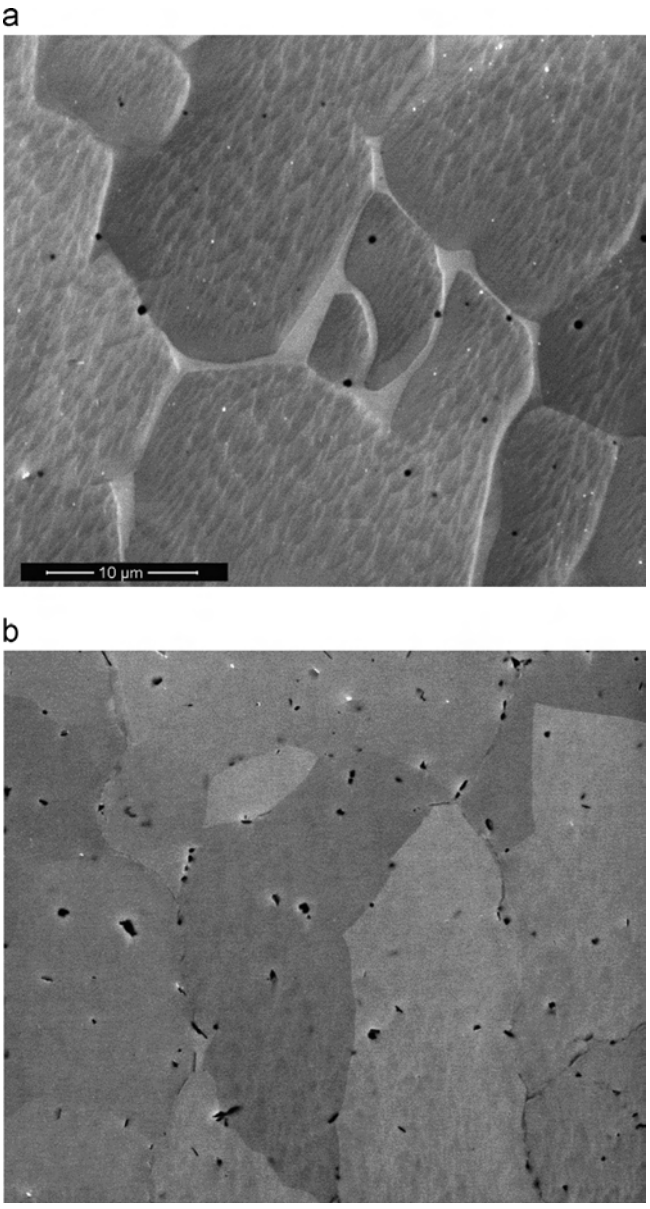

Fig. 3. Photomicrograph of 201 stainless steel (a) as cast and (b) after simulated coiling.

also observed, but not all grains showed this behavior. The 201 stainless was again quite different to the other two alloys, and this composition showed much more homogenous nucleation with a much higher density compared to the other two alloys.

Fully recrystallized microstructures for the three alloys are shown in Fig. 9. The austenitic and ferritic alloys showed an inhomogeneous grain size and grain shape in the fully recrystallized condition. In the case of the ferritic alloy, the prior deformed grain boundaries can be clearly seen in the fully recrystallized structure due to the inhomogeneity of grain development during recrystallization. Clearly, the orientation of the deformed grain had a significant impact on the recrystallized behavior in this case. The austenitic steel showed a similar effect, but the range of grain sizes developed was not as large as in the ferritic case. The 201 stainless steel sample showed a relatively homogenous grain size distribution in the fully recrystallized condition, with an average grain size of ~4 μm. This alloy also showed prolific annealing twins which assisted in reducing the effective grain size of the alloy.

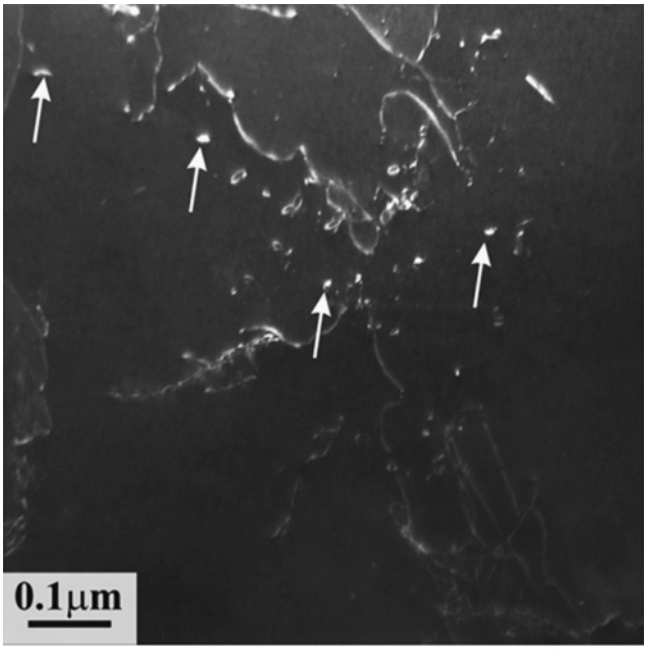

Fig. 4. TEM dark field micrograph of the austenitic stainless steel in the as-cast condition.

3.4. Recrystallization kinetics

The recrystallization kinetics have been examined using the JMAK approach [10]. This model estimates the volume fraction using the equation below:

$$X(t) = 1 - \exp(-kt^n) \quad (1)$$

where t is the annealing time, k is a constant and n is often referred to as the JMAK exponent.

The recrystallization kinetics of the as-cast and coiled samples for an annealing temperature of 850 °C are shown in Fig. 10. For the 201 alloy, an additional annealing temperature of 750 °C was used because the 850 °C recrystallization was too rapid to analyze accurately, with the recrystallization being complete in under 20 s, Fig. 10c. In the case of the austenitic and ferritic stainless steels, a significant delay in recrystallization of the as-cast samples in comparison with the coiled samples is observed. However, the opposite behavior was observed for the 201 stainless steel, with a slight decrease in the recrystallization kinetics being found after coiling.

The calculated values of k and n from the JMAK equation for the three different alloys are shown in Table 3. Note that the values for the 201 series stainless refer to an annealing temperature of 750 °C, whereas the austenitic and ferritic alloys are for an annealing temperature of 850 °C. Also included in this table are the values of k assuming a JMAK exponent of 1, here referred to as k'. This is included here because the JMAK exponent of steels are often found to be close to 1, so we report this here to enable the reader to benchmark against other studies.

4. Discussion

4.1. Recrystallization kinetics

The simulated coiling had a significant effect on increasing the recrystallization kinetics of both the austenitic and ferritic stainless steels. TEM analysis revealed that in the as-cast state, the alloys contained fine particles which were coarsened by the coiling

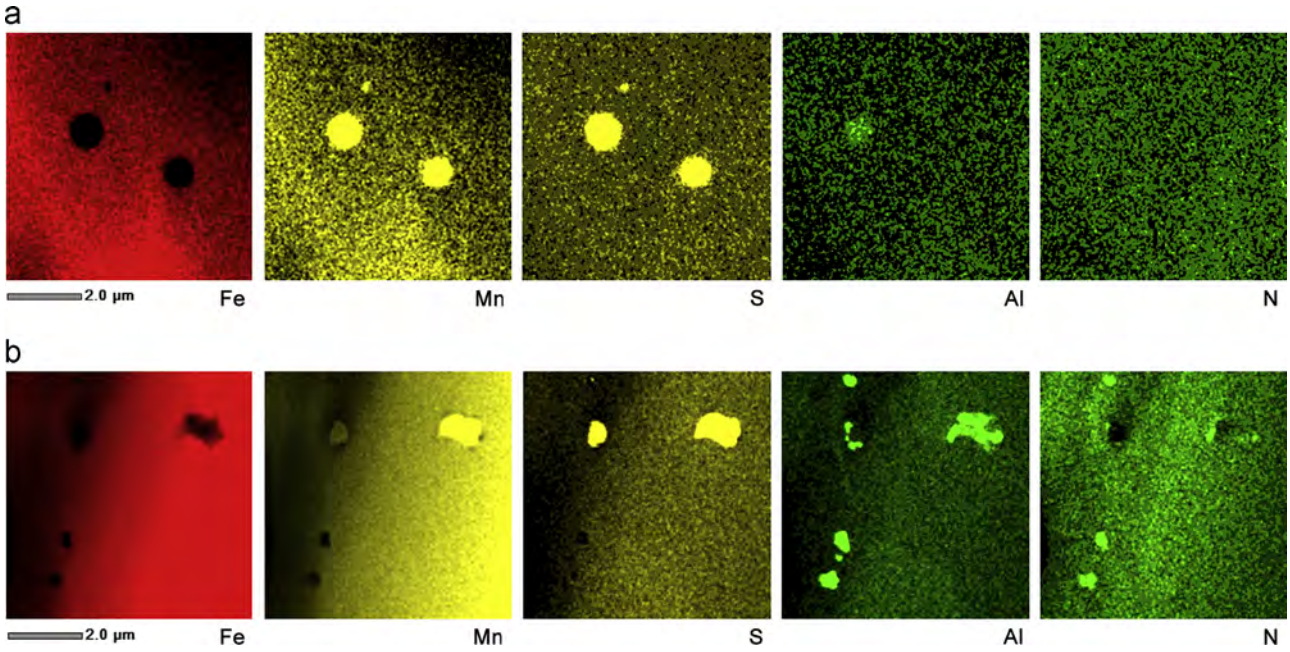

Fig. 5. TEM composition mapping using EDS of the 201 stainless steel and (a) the as-cast condition and (b) after simulated coiling.

Table 2
Summary of the particle size range observed for the three different steels during TEM analysis.

Alloy	Particle type	Size range observed	
		As-cast condition	Coiled condition
Ferritic steel	Complex nitro-sulfide	0.1–0.5 μm	0.4–1 μm
Austenitic steel	Sulfide	Sparse particles 10–30 nm	Sparse particles 0.3–1.2 μm
201 duplex steel	Sulfide	0.2–1.2 μm	0.5–1.3 μm
	Nitride	None observed	0.2–1.6 μm

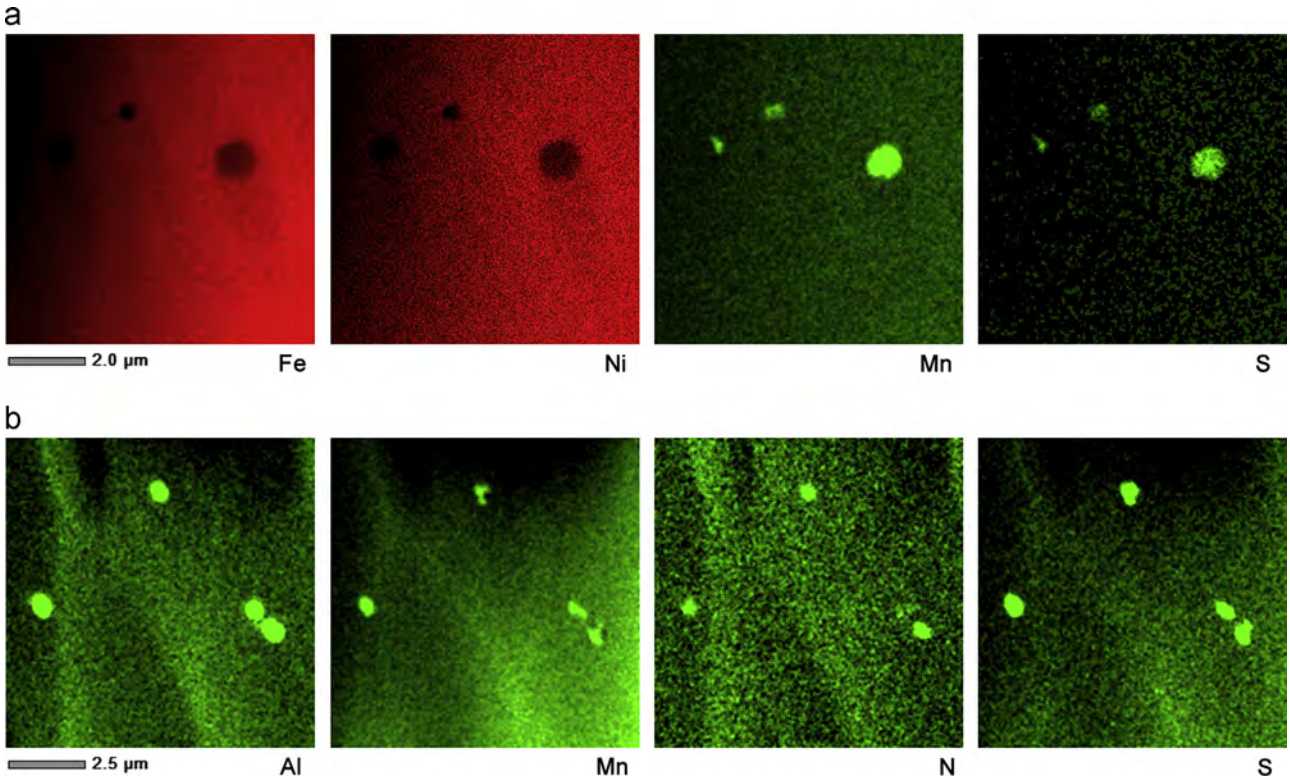

Fig. 6. TEM composition mapping using EDS of the particles developed after coiling of the austenitic and ferritic alloys.

treatment. It is likely that the fine particles pinned the grain boundaries and inhibited grain growth from the as-cast state, while the coiled alloys with their coarsened particles are subject to less grain boundary pining effects. The magnitude of the pinning force can be estimated from the Zener Pinning equation [10]:

$$P_z = \frac{3f_v\gamma}{2r} \tag{2}$$

where P_z is the Zener pinning force, f_v the volume fraction of particles, γ the surface tension of the grain boundary per unit area and r the particle radius.

This can give us a good approximation of what effect particle coarsening will have on grain boundary pinning, and is easily calculable as long as the volume fraction is known. For the case of the ferritic steel, the particle size increases from ~200 nm to ~800 nm as a result of the coiling treatment, although a range of particle sizes was observed. This reduces the average pinning force on recrystallizing boundaries to about one quarter of the original force. This is likely to be the cause of the change in recrystallization kinetics for the two different conditions. For the case of the austenitic steel, the change in particle size was much more marked, nearly an order of magnitude, as a result of simulated coiling. Despite this change in particle size, the difference in recrystallization kinetics between the as-cast and coiled conditions was not as marked as it was for the ferrite. Although we did not quantitatively measure the number of particles per unit volume in this study, we did observe qualitatively that there were much fewer particles in the austenitic steel compared to the other two alloys. This is likely to explain the reduced dependence of recrystallization kinetics on particle size for the austenitic alloy.

The situation for the 201 steel is complicated by the fact that during the coiling, not only do the sulfide particles coarsen, but new nitrides precipitate out from the super-saturated alloy. The coarsened sulfides will have a lower pinning force after coiling, but the increase in volume fraction of the nitrides will add an additional pinning force. Another factor to consider is that the grain boundary length is slightly decreased after coiling due to grain growth, which will likely contribute to a slight decrease in the recrystallization kinetics. The situation is further complicated by the dissolution of delta ferrite into the austenite matrix during coiling, which will both reduce the phase/grain boundary area but also increase solute drag during recrystallization. In the case examined here, these

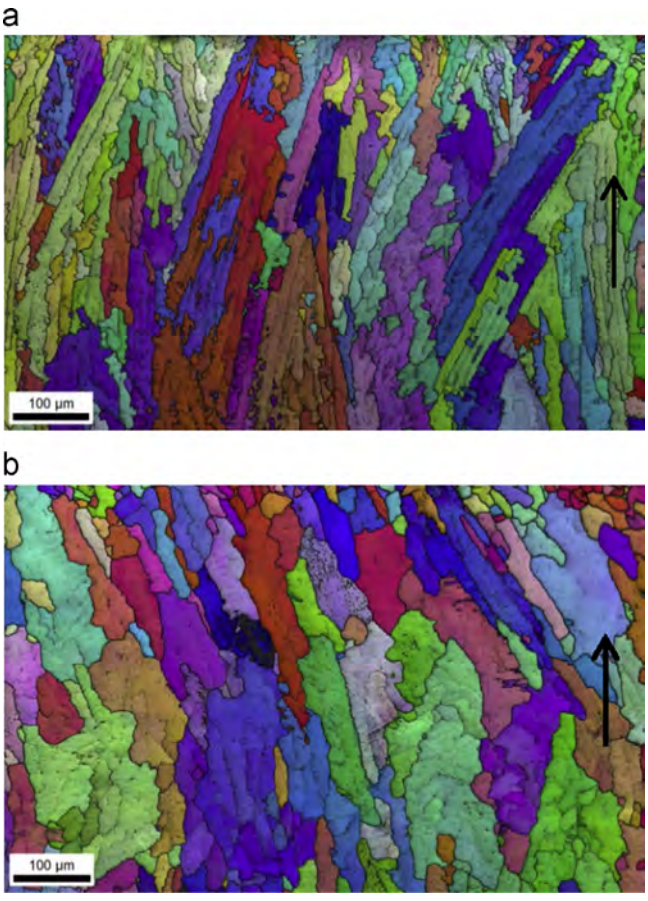

Fig. 7. EBSD micrographs of (a) as-cast and (b) simulated coiling 201 stainless steel. Black arrows show solidification direction.

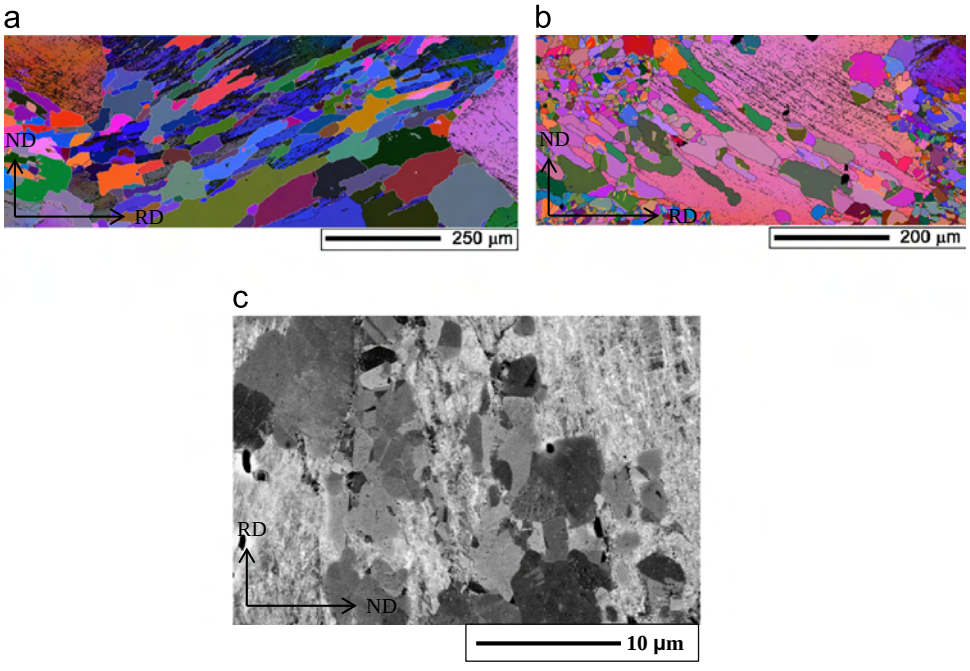

Fig. 8. Partially recrystallized microstructure of (a) Ferritic stainless steel Grain boundaries $>2^\circ$ shown in black, Grain boundaries $>10^\circ$ shown in grey, (b) Austenitic stainless steel Grain boundaries $>2^\circ$ shown in black, Twin boundaries shown in yellow and (c) 201 stainless steel. Note higher magnification in (c).

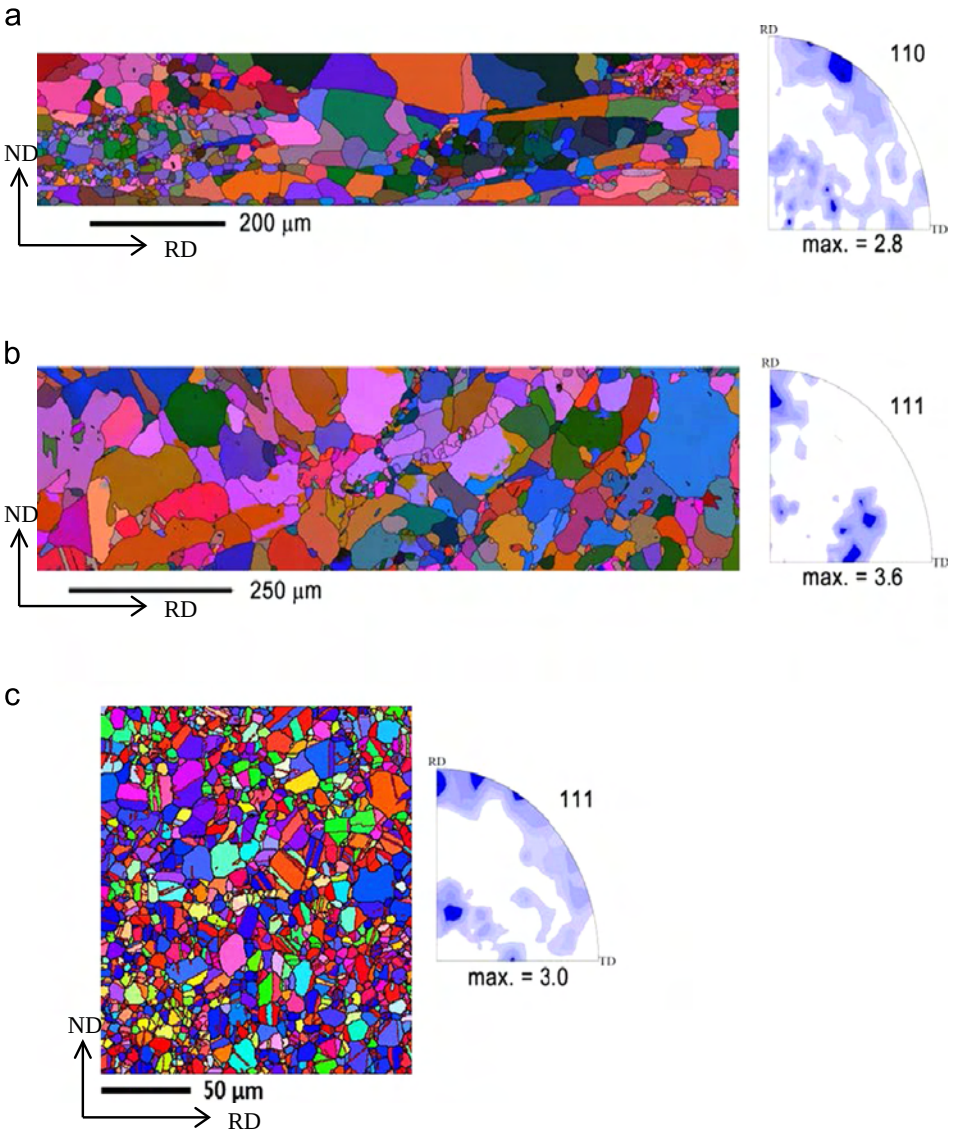

Fig. 9. Fully recrystallized microstructure and corresponding recrystallization textures of (a) Ferritic stainless steel, (b) Austenitic stainless steel, and (c) 201 stainless steel (twin boundaries shown in red).

factors have essentially balanced one-another, leading to only a very small decrease in the recrystallization kinetics of this alloy after simulated coiling. Although the effect was only small in this case, it does highlight that for strip cast steels, precipitation of nitrides during a heat treatment or coiling could produce a microstructure with significantly retarded recrystallization. This is in contrast to the sulfide coarsening where a similar heat treatment does the opposite, and increases recrystallization kinetics. It is clear therefore that the secondary processing of steels after rapid solidification will be alloy chemistry dependant. Where the goal is to recrystallize the alloy to produce a refined grain structure, some alloys will require a coarsening heat treatment to promote recrystallization, while for other alloy chemistries (particularly those susceptible to nitride precipitation) a heat treatment or coiling should be avoided prior to recrystallization.

4.2. *Morphology and texture of recrystallized grains*

Cold rolling and annealing has led to a significant refinement in the microstructure of the as cast samples, as can be seen by comparing Figs.1 and 9. However for the case of the austenitic and ferritic alloys the recrystallized grain size and shape were very inhomogeneous, particularly in the case of the ferritic structure, Fig. 9a and b. This is likely to arise from the fact that the starting grain size was relatively coarse, and that each different starting grain will deform differently in response to cold rolling leading to development of different stored energy in different grains. It is known that two prominent texture components are developed during cold rolling of ferrite, the so-called γ-fiber and α-fiber components, and these two components respond to recrystallization differently [19–21]. Grains oriented along the γ-fiber develop higher stored energy during deformation [22] and consequently exhibit a higher density of nucleation sites during recrystallization. Grains belonging to the α-fiber texture component have a lower stored energy and much lower recrystallization rate. These behaviors are manifested in the present case by the development of regions within the microstructure of the ferritic sample that show a large range of grain sizes and shapes. This effect is so prominent that in the example shown in Fig. 9a the prior deformed grain boundaries which existed prior to recrystallization

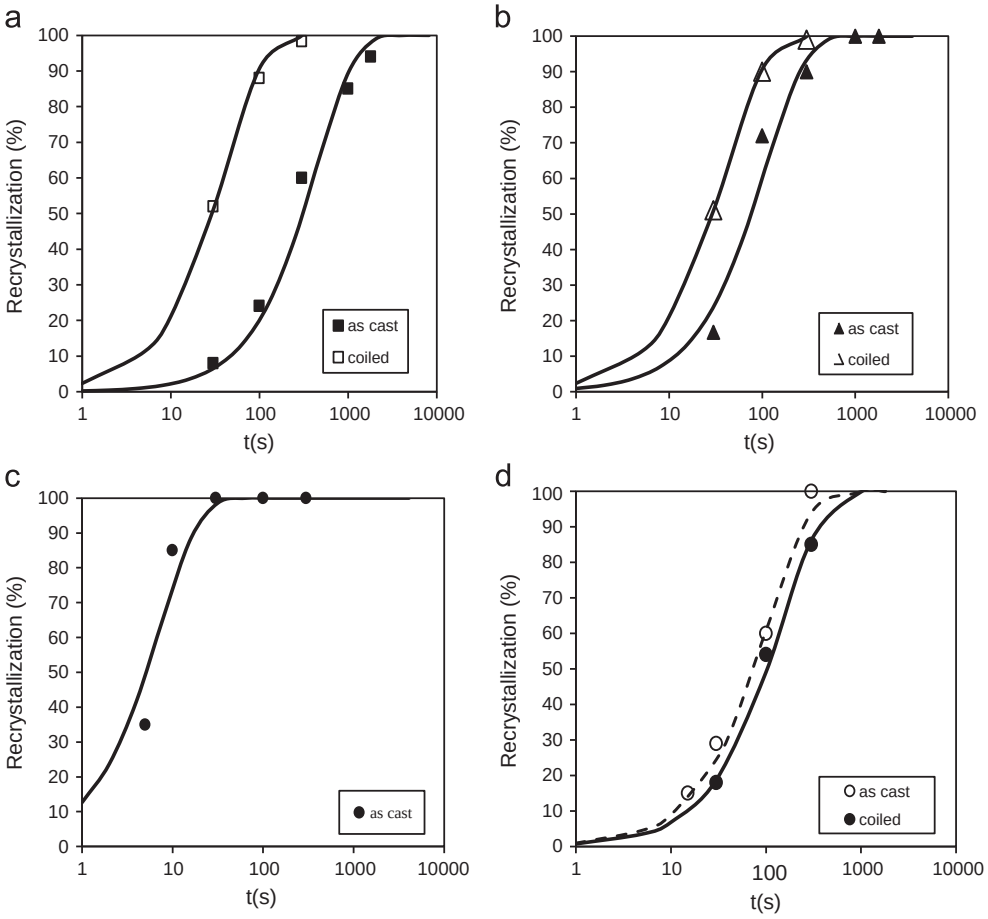

Fig. 10. Recrystallized fraction as a function of time at $T=850$ °C for (a) Ferritic stainless steel, (b) Austenitic stainless steel, (c) 201 stainless steel and (d) 201 stainless steel at $T=750$ °C.

Table 3
Parameters from the JMAK equation for each of the alloys tested. The first two columns show the measured k and n values, whilst k' describes the value of k when n is assumed to be 1.

Alloy	k	n	k'
Austenitic	0.0051	1.1	0.0091
Austenitic (coiled)	0.048	0.8	0.024
Ferritic	0.0051	0.86	0.0022
Ferritic (coiled)	0.061	0.75	0.024
201 stainless	0.015	0.9	0.0093
201 stainless (coiled)	0.0074	0.98	0.0068

can be elucidated. It is evident that some deformed grains showed extensive nucleation and produced regions of fine recrystallized grains. Other deformed grains appear to be nucleation limited, and are consumed by a small number of grains that grow to be quite large. There was not a large enough number of grains in the EBSD map to make a quantitative assessment of the recrystallization texture, Fig. 9a, but the shape of the texture is consistent with recrystallization textures reported for BCC steels [10].

For the austenitic steel also, the recrystallized grain size and shape are inhomogeneous, and the boundaries of the prior deformed grains can be seen in the fully recrystallized microstructure, Fig. 9b. Here too the nucleation of recrystallization has been inhomogeneous throughout the structure, and the orientation of the prior deformed grains has had an impact on the microstructural development, although the disparity on grain sizes is not as marked in the austenite as it was in the ferrite. Here too the texture development could not be quantitatively assessed due to the small sample sizes, but qualitatively the recrystallization textures appear to be consistent with those expected of FCC alloys such as brass [10], Fig. 9b.

The finest grain size distribution was obtained in 201 stainless steel (Fig. 9c). This alloy showed the most rapid recrystallization, which is likely to be the result of its much finer starting microstructure. This is also likely to contribute to the much more homogenous nucleation observed in this alloy. The recrystallization texture that developed was similar to the deformation textures that are developed during rolling of FCC metals, Fig. 9c.

In conclusion, it is worth benchmarking the present microstructures against those that would be found in commercially produced materials. In the ferritic and austenitic alloys studied here, the cold rolling and annealing procedure has reduced the grain size by about an order of magnitude. However, the microstructures remain more coarse and more inhomogeneous than would be achieved through traditional thermo-mechanical processing of a cast slab. This is largely due to the limitation of casting a thin strip, a maximum reduction of ~50% can be applied during rolling compared to the reductions of over 95% that can be applied to a thick slab during its processing into sheet. The multiple deformation and recrystallization steps that are possible during the processing of a slab enable the microstructure to go through multiple refinement and homogenization cycles. In the case of strip cast materials, there is only one opportunity to refine the microstructure by recrystallization. Particularly in the case of the ferritic alloy, this single deform-and-anneal cycle did not produce a homogenous microstructure. The case of the 201 stainless alloy

was quite different. As a consequence of its phase transformation during cooling, this alloy was relatively fine in the as-cast condition. After an additional rolling and annealing procedure, the high grain boundary area in the starting structure aided in the refinement that was achieved during recrystallization by providing a high density of potent nucleation sites. This alloy therefore developed a fine and homogenous microstructure from a single recrystallization treatment. Clearly, choosing an alloy chemistry that utilizes the austenite to ferrite phase transformation during strip casting can provide significant scope for microstructural refinement in both the as-cast and annealed conditions.

5. Conclusions

The microstructural development of three different strip cast stainless steels following cold rolling and annealing were investigated in the present study. The main results are as follows:

- The rapid solidification associated with strip casting develops very fine precipitates in the microstructure of the as-cast samples. For the three alloys sulfide particles were present in the as-cast structure, and these exhibited a relatively wide range of sizes.
- Alloys were subjected to a simulated coiling treatment. This resulted in the coarsening of the particles present in the austenitic and ferritic alloys, and these were identified to be sulfides. In the 201 series stainless, the existing sulfides were coarsened by the coiling treatment, and this was also accompanied by precipitation of aluminum nitrides which were not present in the as-cast structure.
- For the ferritic and austenitic alloys, the recrystallization of the cold rolled microstructure was significantly slower in the as-cast state due to the fine precipitates that were present. However, those samples subjected to the simulated coiling treatment had coarsened particles, and the recrystallization rate was increased due to a reduction in particle pinning of the boundaries of the recrystallized grains.
- The strip cast 201 stainless steel, however, behaved differently in terms of recrystallization kinetics and the as-cast samples showed slightly accelerated recrystallization compared to the coiled sample. The slightly retarded recrystallization kinetics in the coiled condition has been attributed to three changes that occurred during coiling: the formation of aluminum nitride precipitates, a small amount of grain growth, and the dissolution of delta ferrite leading to an increase in solute drag.
- Very fine manganese sulfides can be produced during rapid solidification, and these can lead to significantly retarded recrystallization. This can be alleviated through a heat treatment process to coarsen the precipitates.
- For the case of aluminum nitrides, these remain in solution during rapid solidification and only appear in the microstructure after a heat treatment. In the case studied here these were responsible for only a small decrease in the recrystallization kinetics, but this effect could be significantly more potent for heat treatments in which the precipitates become much finer. For recrystallization of steel chemistries that are susceptible to AlN formation, heat treatments should be avoided after rapid solidification in order to avoid precipitation.
- Even though all of the alloys were successfully cold rolled and fully recrystallized, this treatment in two from the three alloys produced an inhomogeneous grain size distribution, and a relatively large grain size compared to that which would be obtained from thermo-mechanical processing of a conventional thick slab casting. Only the 201 stainless alloy produced a fine and homogenous recrystallized microstructure, and this has been attributed to the much finer as-cast structure developed in this particular alloy.

Acknowledgments

The work carried out in this paper was funded by the Australian Research Council's Discovery Grant scheme (DP0879319) and the Laureate Fellowship Grant (FL0992361). The technical assistance of Andrew Sullivan, Rosey Van Driel, Dave Gray, Mohan Setty and Lynton Leigh is gratefully acknowledged. The authors would also like to make special mention of the support provided by The Crucible Group, in particular Dr K. Mukunthan, during the casting stages of this research.

References

[1] M. Ferry, Direct Strip Casting of Metals and Alloys, Woodhead Publishing Limited, Cambridge, UK & CRC Press LLC, New York, USA, 2006.
[2] L. Strezov, J. Herbertson, G.R. Belton, Metall. Mater. B 31B (2000) 1023–1030.
[3] Z. Liu, Y. Kobayashi, K. Nagai, ISIJ Int. 44 (2004) 1560–1567.
[4] K. Hirata, O. Umezawa, K. Nagai, Mater. Trans. 43 (2002) 305–310.
[5] Z. Liu, Y. Kobayashi, K. Nagai, J. Yang, M. Kuwabara, ISIJ Int. 46 (2006) 744–753.
[6] L.D. Frawley, R. Priestner, Mater. Sci. Forum 284–286 (1998) 485–492.
[7] K. Xie, L. Yao, C. Zhu, J. Cairney, C. Killmore, F. Barbaro, J. Williams, S. Ringer, Metall. Mater. Trans. A 42 (2011) 2199–2206.
[8] C. Zener quoted in C.S. Smith, Trans. Metall. Soc. AIME 175 (1948) 15–51.
[9] P.A. Manohar, M. Ferry, T. Chandra, ISIJ Int. 38 (1998) 913–924.
[10] F.J. Humphreys, M. Hatherly, Recrystallization and Related Annealing Phenomena, 2nd edition, Elsevier, Oxford, 2004.
[11] W. Xu, M. Ferry, Journal of Materials Processing Technology 203 (2008) 518–525.
[12] M. Arribas, B. López, J.M. Rodriguez-Ibabe, Mater. Sci. Eng. A 485 (2008) 383–394.
[13] L. Strezov, J. Herbertson, ISIJ Int. 38 (1998) 959–966.
[14] K. Mukunthan, P.D. Hodgson, P. Sellamuthu, L. Strezov, Y. Durandet, N. Stanford, ISIJ Int., this issue.
[15] K. Mukunthan, P.D. Hodgson, L. Strezov, N. Stanford, ISIJ Int., this issue.
[16] K. Mukunthan, P.D. Hodgson, P. Sellamuthu, L. Strezov, Y. Durandet, N. Stanford, Under review.
[17] A. Hunter, M. Ferry, Scr. Mater. 47 (2002) 349–355.
[18] B. Chalmers, Principles of Solidification, John Wiley & Sons, New York, 1967.
[19] C.W. Sinclair, F. Robaut, L. Maniguet, J. Mathieux, J. Schmitt, Y. Brechet, Adv. Eng. Mater. 5 (2003) 570–574.
[20] E. Lindh, B. Hutchinson, P.S. Bate, Mater. Sci. Forum 157–162 (1994) 997–1002.
[21] I. Samajdar, B. Verlinden, L. Kestens, P. Van Houtte, Acta Mater. 47 (1999) 55–65.
[22] B. Hutchinson, Philos. Trans. R. Soc. Lond. A 357 (1999) 1471–1485.